Flutter Analysis of Cantilever Composite Plates in Subsonic Flow

Kuo-Juin Lin,* Pong-Jeu Lu,† and Jiann-Quo Tarn‡
National Cheng Kung University, Tainan, Taiwan, Republic of China

The high-precision 18-degree-of-freedom triangular plate-bending finite element is used to study the effects of composite filament angle, orthotropic modulus ratio, sweep angle, and aspect ratio on the vibration and flutter/divergence characteristics of cantilever plates in subsonic flow. The element stiffness and mass matrices are generated according to the classical lamination theory. Unsteady airload acting on the plate is evaluated by the use of lifting surface theory, which is solved numerically by the doublet-lattice method. To facilitate flutter analysis, interpolation using a surface spline is employed to interconnect the structural nodal and aerodynamic control points. The flutter/divergence tradeoff of aeroelastic tailoring is found, in a more involved manner, for the present plate-like low-aspect-ratio wings as compared to that associated with the beam model first discovered by Weisshaar. Effective enhancement on flutter/divergence performance can be attained by varying the orthotropic modulus ratio while as appropriate fiber orientation is selected. Also, as discovered previously, the present numerical results confirm that the structural tailoring can provide a harmonious balance to the sweep angle effect upon the aeroelastic stability characteristics of a wing. From the numerical examinations performed, it is concluded that substantial improvement upon flutter/divergence characteristics can be achieved by using composite materials. Nevertheless, the benefit can be gained only through a thorough parametric investigation because the aeroelastic stabilities are also complicated by the directional stiffness of composites, in particular for the cases of low-aspect-ratio wings.

I. Introduction

FLUTTER and divergence phenomena are defined respectively as the dynamic or static instability of an aeroelastic system, characterized by the interactions of elastic deformation and aerodynamic loads. They are aeronautically very important since the onset of flutter/divergence may quickly develop into catastrophic structural failure or undesirable limit-cycle oscillations. In addition, the modern aircraft design requiring high speed with lightweight structure makes the aeroelastic analysis a stringent necessity in the design stage. Employing composite material in the manufacture of aircraft structure has been one of the avenues to enlarge the flutter/divergence boundary of an aircraft. This is due to the prominent characteristics associated with composite material, namely, the high strength/stiffness-to-weight ratio and the controllable material properties that usually are not possessed by conventional materials. Studies using composite structures to improve the aeroelastic behavior, divergence, or flutter, as termed by aeroelastic tailoring, have been conducted by many researchers, and all investigations confirmed the benefit of composite material in enhancing the aeroelastic properites.[1-11] Reference 1 presents an excellent review of aeroelastic tailoring and many useful references are listed therein.

Weisshaar[2,3] employed laminated box beam theory and two-dimensional, incompressible strip aerodynamic theory to predict the divergence characteristics of swept wings. He concluded that the bending-torsion stiffness coupling of anisotropic composite materials could be used to alleviate divergence for a large range of forward sweep angles. This conclusion was verified in wind-tunnel tests by both Sherrer et al.[4] and Blair and Weisshaar.[5] Weisshaar's model was further adopted for flutter analysis by Lehman[6] and Lottati.[7] Lehman showed that a strong dependence of composite filament angle was found for the flutter characteristics. Lottati discovered that the effect of bending-torsion stiffness coupling makes a compromise between flutter and divergence characteristics for various sweep angles. For plate-like wings, Rogers et al.[8] and Braymen et al.[9] performed work in the aeroelastically tailored lifting surfaces concerned mainly with static aerodynamic improvements. In spite of their efforts, the amount of analytical and experimental investigations put forward for flutter characteristics of plate-like composite wings has been very limited. Recently, a series of investigations for both the divergence and flutter behaviors of composite cantilever plates were conducted by Hollowell and Dugundji[10] and Landsberger and Dugundji.[11] The analytic investigation used a Rayleigh-Ritz formulation together with incompressible three-dimensional Weissinger L-method aerodynamics for the divergence and an incompressible two-dimensional unsteady strip theory for the flutter. The results indicated that divergence and bending-torsion flutter appear at low angles of attack, whereas torsion and bending stall flutter occur at higher angles of attack.

The present work attempts to develop a more general approach for the flutter analysis of plate-like composite structures (divergence can be considered as a special case of flutter). A high-precision triangular finite-element method is used to discretize the structure, while bearing in mind that the finite-element method is more versatile in treating general complex geometries. Three-dimensional, unsteady compressible lifting-surface theory and the doublet-lattice method are adopted for the evaluation of aerodynamic forces. The emphasis of the present study is placed on the methodology development, although a simple plate-like composite structure is assumed for the structural model. Therefore, the extension of the present method to more practical structures can be straightforward. The effects of composite filament angle, orthotropic modulus ratio, aspect ratio, and wing sweep angle on the vibration and flutter characteristics of a composite cantilever plate in subsonic flow are examined numerically. The flutter/divergence tradeoff discovered in the present results for low-aspect-ratio wings is found in a more involved manner than that found for the beam-like wings. Other effects associated with the composite material parameters and the wing geometric shapes were also investigated and explained. It

Received June 18, 1987; revision received Aug. 30, 1988.

*Graduate Research Assistant, Institute of Aeronautics and Astronautics.
†Associate Professor, Institute of Aeronautics and Astronautics.
‡Professor and Chairman, Department of Civil Engineering.

was found that substantial improvement on the flutter/divergence performance of wings can be achieved if the composite plate is properly tailored.

II. Analysis

A. Hamilton's Principle for a Nonconservative System

The derivation of the equations of motion for flutter analysis is most conveniently obtained through the use of Hamilton's principle. Employing Hamilton's principle for a nonconservative elastic system would result in the following variational form that governs the dynamics of the system:

$$\delta\int_{t_1}^{t_2} L\,dt + \int_{t_1}^{t_2} \delta W^{NC}\,dt = 0 \tag{1}$$

where L is the Lagrangian defined as $L = T - U$, T the total kinetic energy of the system, U the total potential, or strain energy of the system (the gravitational potential is neglected for the present case), δW^{NC} the virtual work done by the nonconservative force field (for this case, it is the work done by aerodynamic forces), and t_1 and t_2 the initial and final time of the motion.

The Lagrangian L will be deduced in the next section based on the finite-element technique, from which the system mass and stiffness matrices are formulated. As for the virtual work term, δW^{NC}, which involves the use of doublet-lattice method for the unsteady lifting surface theory, the formulation will be explained and shown subsequently in terms of the aerodynamic influence and the transformation matrices in Sec. II.C and D.

B. Structural Finite-Element Discretization

The high-precision 18-degree-of-freedom triangular plate-bending finite element (T18 element) is used here to generate the mass and stiffness matrices associated with the plate-like structure. This method, originally developed by Argyris et al.,[12] Bell,[13] and Cowper et al.,[14] involves a large matrix inversion and numerical integration and hence is very time consuming in application, although it has the advantage being conforming and accurate. Such a drawback in inefficiency was remedied by Stavitsdy et al.[15] via the use of an oblique coordinate system while analyzing creeping flow problem. Recently, Jeyachandrabose and Kirkhope[16,17] succeeded in using this improved method to analyze plate problems and thus reformulated the associated stiffness matrix of the thin plate. It is this improvement that makes the triangular finite element one of the most efficient and reliable thin plate elements. This high-precision triangular element has another property, being geometrically versatile, which is of particular value for developing methods in coping with problems having complex configurations. Based on these reasons, this T18 element technique is employed in the present work to treat the static and dynamic aeroelastic problems of laminated anisotropic plates.

In the following derivation the x,y coordinates and all the deformations are nondimensionalized by the half root chord b_r of the plate. The transverse displacement field w, within a T18 element, can be expressed in the form[16]

$$w = \{\Lambda\}^T[Q]\{q\} \tag{2}$$

where $\{q\}$ is a column vector defined in terms of the generalized coordinates associated with the three vertices of the triangular element,

$$\{q\}^T = \lfloor \hat{q}_1^T\ \hat{q}_2^T\ \hat{q}_3^T \rfloor = \lfloor q_1\ q_2 \ldots q_{18} \rfloor$$

$$\{\hat{q}_i\}^T = \lfloor w_i\ w_{x_i}\ w_{y_i}\ w_{xx_i}\ w_{xy_i}\ w_{yy_i} \rfloor, \qquad i = 1,2,3$$

where $\{\hat{q}_i\}^T$ is composed of the displacement, slopes and curvatures of the element at the ith vertex. The column vector $\{\Lambda\}$ consists of complete quintic polynomial expressed in terms of the oblique coordinates (ξ,η) that guarantees the element to be conforming and is given by

$$\{\Lambda\}^T = \lfloor 1\ \xi\ \eta\ \xi^2\ \xi\eta\ \eta^2 \ldots \xi^5 \ldots \eta^5 \rfloor$$

$[Q]$ is a 21×18 transformation matrix related to the element geometry. The explicit form for $[Q]$ can be found in Ref. 16.

According to the classical lamination theory, the kinetic and strain energy of the structural element made of symmetrically laminated composites are derived as

$$T = \tfrac{1}{2} b_r^4 \rho_s t_s \int\int_\Delta \dot{w}^2\,dx\,dy \tag{3}$$

$$U = \tfrac{1}{2} D_{11} \int\int_\Delta \{\chi\}^T[\bar{D}]\{\chi\}\,dx\,dy \tag{4}$$

In the formulation, ρ_s and t_s are the density and thickness of the plate element, respectively, Δ the area of the element, $[\bar{D}]$ the symmetric flexural rigidity matrix of the laminated plate[18] normalized by the x-axis rigidity D_{11}, and $\{\chi\}$ the curvature vector given by

$$\{\chi\}^T = \lfloor w_{xx}\ w_{yy}\ 2w_{xy} \rfloor$$

Substituting Eq. (2) into Eq. (4), Jeyachandraboses[16] obtained the following form for the strain energy of the element:

$$U = \frac{1}{2}\frac{D_{11}}{(2\Delta)^3}\{q\}^T[Q_1]^T[\bar{F}_1][Q_1]\{q\} \tag{5a}$$

$$[\bar{F}_1] = \frac{1}{D_{11}}\frac{t_s^3}{12}[F_1] \tag{5b}$$

The definitions of matrices $[Q_1]$ and $[F_1]$ are given in Ref. 16.

For the present flutter analysis, one has to derive for the mass matrix to account for the inertia effect. Substituting Eq. (2) into Eq. (3) and after some manipulations, the kinetic energy of the element may be derived in the form

$$T = \tfrac{1}{2} b_r^4 \rho_s t_s (2\Delta)\{\dot{q}\}^T[Q]^T[\bar{\Lambda}][Q]\{\dot{q}\} \tag{6}$$

where the 21×21 symmetric matrix $[\bar{\Lambda}]$ is given by

$$[\bar{\Lambda}] = \int_0^1\int_0^{1-\xi} \{\Lambda\}\{\Lambda\}^T\,d\eta\,d\xi \tag{7}$$

Taking the variation of the time integral of the Lagrangian L, the mass and stiffness matrices of the T18 element can readily be found to be

$$[M]_e = b_r^4 \rho_s t_s (2\Delta)\{Q\}^T[\bar{\Lambda}][Q] \tag{8}$$

$$[K]_e = \frac{D_{11}}{(2\Delta)^3}[Q_1]^T[\bar{F}_1][Q_1] \tag{9}$$

C. Aerodynamic Theory and the Doublet-Lattice Method (DLM)

Unsteady aerodynamic model is known to be very crucial for flutter calculations. In subsonic fluid flows, wake plays a very critical role in the determination of the aerodynamic damping effect. It has been found that an inappropriate aerodynamic model often causes substantial error in flutter analysis.[19,20]

The present work uses the linearized potential flow model that, as a consequence of assuming that the structure is undergoing simple harmonic motion, can be expressed by a singular integral equation connecting the downwash and the pressure distribution on the lifting-surface as

$$\frac{\bar{w}_a}{V}(x,y,z) = \frac{1}{8\pi} \oint\int_s \Delta\bar{C}_p(x_1,y_1,z_1) \times K(x-x_1, y-y_1, z-z_1; k, M)\,dS \tag{10}$$

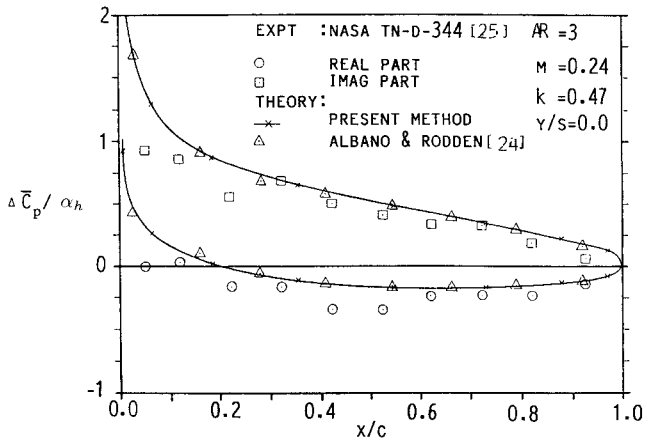

a) At wing root

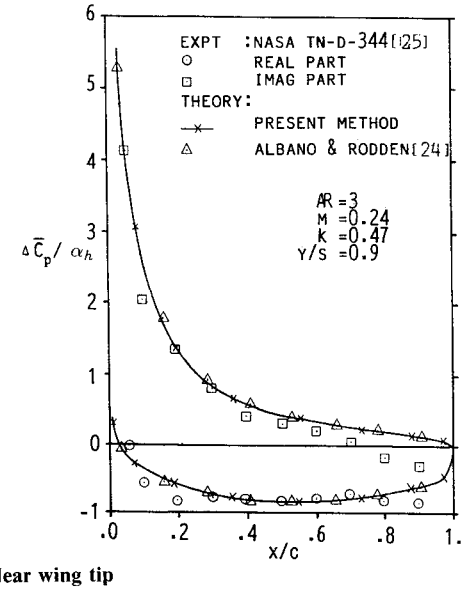

b) Near wing tip

Fig. 1 Lift distribution on rectangular wing oscillating in bending mode.

where s is the wing area, V the freestream velocity, and $\bar{w}_a$ and $\Delta \bar{C}_p$ the downwash and pressure coefficient differential across the wing, respectively. The bar ( ) denotes that the variable beneath is complex valued, carrying information of both magnitude and phase shift, K is the kernel function representing the downwash at a location (x,y,z) induced by a unit impulse load at the position (x_1,y_1,z_1). The form of the kernel function used herein is the one suggested by Landahl.[21]

The unsteady aerodynamic code used for the present flutter problem was developed by Chu and Lu.[22,23] It is a wing-body combination code developed along the line of doublet-lattice method (DLM) together with the interior body singularity method. Several validity tests are performed for a cantilevered wing, and the results are shown in Fig. 1. The comparisons are made with those calculated by Albano and Rodden[24] and those obtained by experiment.[25] The agreements are quite satisfactory in general.

Employing the DLM procedure, the nonconservative virtual work term δW^{NC} contributed from all the aerodynamic elements can be summed up to yield

$$\delta W^{NC} = b_r^3 \{\delta \bar{w}\}^T [\Delta s_j] \{\Delta \bar{p}\} \tag{11}$$

Note that $\{\delta \bar{w}\}$ is the displacement vector evaluated at each control point of the aerodynamic element, and the middle diagonal matrix is defined with the element area Δs_j aligned diagonally.

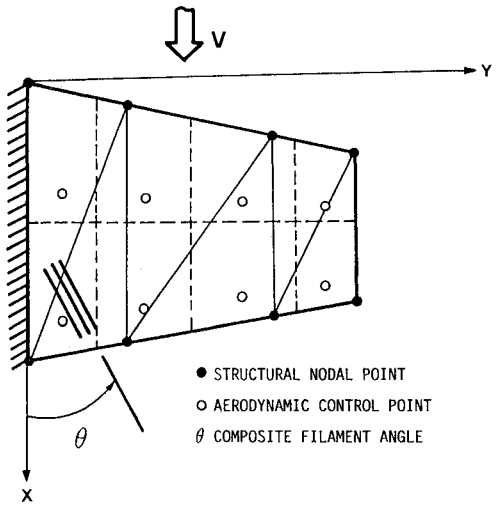

Fig. 2 Structural and aerodynamic networks.

D. Interpolation between Structural and Aerodynamic Networks

The discretization of structural and aerodynamic models usually leads to two sets of nodal and/or control points that form two different networks. Aerodynamic panels, which almost exclusively adopt quadrilateral shapes, must be oriented with their side edges parallel to the airstream direction, owing to the specific physics inherent in discretizing the lifting surfaces. The present work uses triangular finite elements for structures and hence results in a different set of locations of the nodal points as opposed to those of the aerodynamic control points. A schematic is illustrated in Fig. 2. Among various methods used in interconnecting these two networks, the one developed by Harder and Desmarais[26] proves to be the most successful. The interpolation function used by Harder and Desmarais is the surface spline function derived from an infinite thin plate pinned at the fitting points. Physically, this is equivalent to making the mathematical interpolation between the fitting points more compatible with the actual deflection of the structures. Therefore, the downwash at the aerodynamic control points, as derived from this interpolation function, can be more accurately approximated, and the spurious wriggles that may result in a completely erroneous evaluation of the air loads acting on the structure can be avoided.

The detail derivation of the interpolation function is elaborated in Ref. 26. The relation between the locations of the aerodynamic control points and the structural nodal points can be established using some transformation matrices $[T_1]$ and $[T_2]$, which, as inserted into the expression of $\{\delta \bar{w}\}$ and $\{\Delta \bar{p}\}$, yields the nonconservative virtual work δW^{NC} of the form

$$\delta W^{NC} = \tfrac{1}{2} b_r^3 \rho_a V^2 \{\delta \bar{q}\}^T [\tilde{A}] \{\bar{q}\} \tag{12a}$$

$$[\tilde{A}] = [T_1]^T [\Delta s_j] [A]^{-1} (ik[T_1] + [T_2]) \tag{12b}$$

where ρ_a is the air density and $[A]^{-1}$ the inverse of the aerodynamic influence coefficient matrix. The detail derivation leading to Eqs. (12) can be found in Ref. 27.

E. Flutter Equations and Solution Method

Assembling together the previously derived element mass and stiffness matrices of the structure and the aerodynamic force acting on it, the equations of motion can be obtained. Furthermore, by adopting the assumption of simple harmonic oscillation, for which the onset of flutter is defined, the flutter equations can be derived as

$$\left(-\lambda^2[M] + [K] - \frac{1}{2}\frac{b_r^3 \rho_a V^2}{D_{11}} [\tilde{A}]\right)\{\bar{q}\} = \{0\} \tag{13}$$

Table 1 Nondimensional natural frequency λ of isotropic square cantilevered plate ($\nu = 0.3$)

	Mode				
Element division	1st	2nd	3rd	4th	5th
T18—2 × 2	0.8713	2.1314	5.3296	6.8180	7.7713
T18—3 × 3	0.8695	2.1290	5.3267	6.8047	7.7506
T18—4 × 4	0.8688	2.1283	5.3253	6.8013	7.7456
Srinivasan[28]	0.8698	2.1403	5.3193	6.7918	7.7608
Young[28]	0.8735	2.1368	5.3600	6.8650	7.7925
Claasen[28]	0.8675	2.1375	5.3225	6.8000	7.7750

Table 2 Natural frequencies (Hz) λ of cantilevered laminated plate for model $[0_2/90]_s$

	Mode				
Element division	1st	2nd	3rd	4th	5th
T18—1 × 4	11.055	39.566	69.260	132.664	193.938
T18—2 × 8	11.053	39.544	69.255	132.535	193.926
T18—3 × 12	11.053	39.542	69.253	132.519	193.923
Ref. 10 theory	10.7	39	67	132	430
Ref. 10 expt	11.1	42	69	—	—

in which λ is a nondimensional frequency

$$\lambda^2 = \omega^2 b_r^4 (\rho_s t_s / D_{11}) \tag{14}$$

Note that the boundary conditions associated with the cantilever plate, namely,

$$w = w_x = w_y = w_{xx} = w_{xy} = 0 \qquad \text{at } y = 0 \tag{15}$$

have already been taken care of in the derivation of the flutter equations [Eq. (13)].

The *V-g* method is adopted for solving these flutter equations. In order to facilitate the *V-g* method procedure, a modal analysis of the free vibration, i.e., ignoring the aerodynamic forcing term, ought to be performed first to diagonalize the mass and stiffness matrices. In doing so by pre- and postmultiplying the flutter equations with the associated modal matrix $[\Phi]$ and introducing in a parameter g, which is analogous to the structural damping, the *V-g* method flutter equations can be obtained as

$$\left([I] + \frac{m^*}{2k^2} [\bar{A}(k, M_0)] - Z[\lambda_s^2] \right) \{\tilde{q}\} = 0 \tag{16}$$

where

$$\{\tilde{q}\} = [\Phi]^{-1} \{\bar{q}\}$$

$$m^* = \rho_a b_r / \rho_s t_s$$

$$[\bar{A}] = [\Phi]^T [\tilde{A}] [\Phi]$$

$$Z = (1 + ig)/\lambda^2$$

$$\lambda_{s_i}^2 = \omega_i^2 b_r^4 (\rho_s t_s / D_{11})$$

and the ω_i are the natural frequencies of the cantilever plate.

It is commonly understood that an accurate determination of the structural natural frequencies is a necessary prerequisite for the flutter analysis. To check for this, a free vibration analysis is first carried out, and the comparisions of the results with others are listed in Tables 1 and 2. In Table 1, the structure is an isotropic square cantilever plate, and the methods used by Srinivasan, Young, and Claasen (see Ref. 28) are all analytic. Agreement among the data is very good in general. Table 2 shows the results obtained for a composite cantilever plate. Except for the fifth mode, good agreement in the data obtained by those using the present T18 element method and by the MIT group[10] can be observed. In both of these examinations, the T18 element method exhibits the very appealing property of a quick, monotonically decreasing convergent rate with increasing element numbers for all the natural frequencies. This feature of the T18 element method indicates that, at least for plate-like structures, the triangular finite-element approach makes a good candidate for analyzing composites.

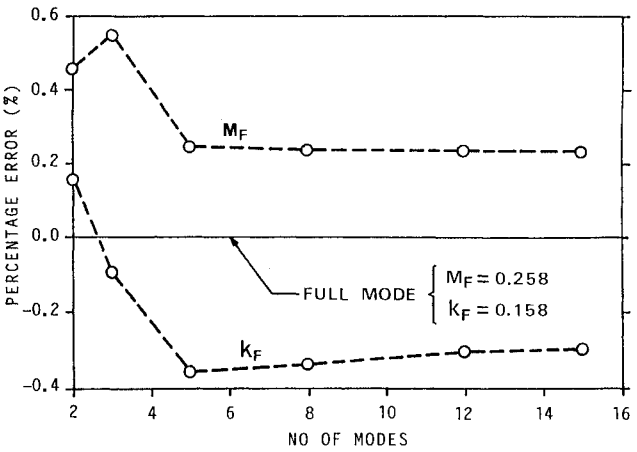

Fig. 3 Flutter solutions vs number of modes ($AR = 4$, $\beta = 8$, $\theta = 0$ deg, $M_0 = 0.3$, structural mesh = 3 × 4, aerodynamic mesh = 6 × 6).

Solving the resultant flutter system [Eq. (16)], is very time consuming. The reason is that the T18 element may easily generate a system of very large degrees of freedom. This inefficiency would deteriorate, especially when adding the calculation of the aerodynamic loads and the necessity required for the *V-g* method to search a wide spectrum of trial Mach numbers M_0 to locate the genuine flutter speed. Fortunately, most wing flutter phenomena are due to lower-mode instability. Therefore, by using a reduced system pertaining to the full-mode system, including only the lowest modes, the computing effort can be significantly reduced without sacrificing too much in accuracy. An example is shown in Fig. 3, which illustrates the percentage error resulted from using reduced degree-of-freedom systems. The structural and air properties taken for this examination of a unidirectional composite plate fluttering in air are listed below:

$E_T = 0.4 \times 10^{10}$ N/m^2 $\qquad \nu_{LT} = 0.25$

$G_{LT} = 0.4\, E_T$ $\qquad \beta = E_L/E_T$

$\rho_s = 1500$ kg/m^3 $\qquad t_s = 0.016$ m

$b_r = 0.5$ m $\qquad \rho_a = 0.45908$ kg/m^3

Sound speed = 303.2 m/s

where ν_{LT} is the longitudinal Poisson's ratio and E_L, E_T, and G_{LT} the longitudinal and transverse Young's moduli and the longitudinal shear modulus of unidirectional composites, respectively. The parameter β is defined as the orthotropic modulus ratio and $\beta = 1$ corresponds to an isotropic plate. For a test case of the low-aspect-ratio plate ($AR = 4$) shown in Fig. 3, the errors associated with the flutter speed and flutter frequency using five modes are within 0.3 and 0.4%, respectively. These results confirm that five modes are generally sufficient; therefore, all subsequent parametric studies of flutter experiments use five modes for the calculations.

The relationships of the calculated flutter Mach numbers vs the trial Mach number, which are preset in the calculation of the aerodynamic influence coefficients, are shown in Fig. 4.

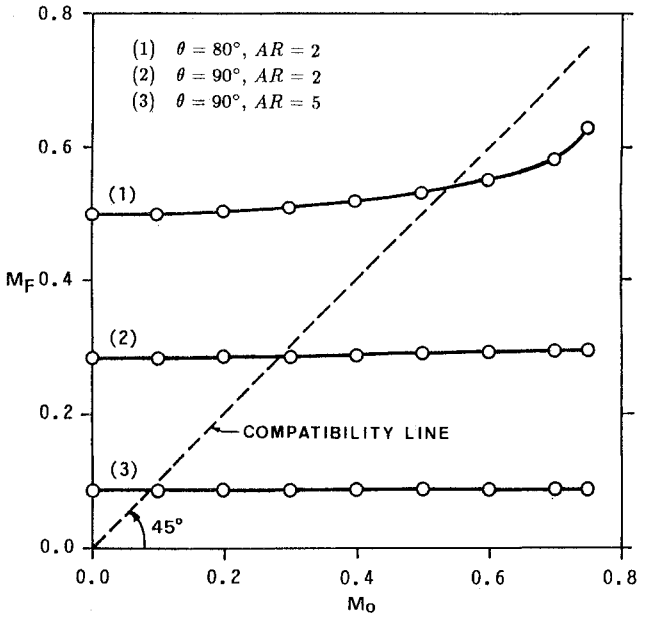

Fig. 4 Flutter Mach number vs trial Mach number ($\beta = 8$, number of modes = 5, structural mesh = 3 × 4, aerodynamic mesh = 6 × 6).

Table 3 Check of the flutter solutions of composite cantilevered plate

	Composite laminated models			
	$[0_2/90]_s$		$[30_2/0]_s$	
Solution	V_F, m/s	f_F, Hz	V_F, m/s	f_F, Hz
Ref. 10 expt	25	29	27	28
Ref. 10 comp	21.0	25	27.8	31
Present	21.8	25.6	24.9	26.4

For a given altitude, only the intersecting points of the flutter curves and the line of compatibility relation are physically meaningful. The flutter velocities stated hereafter are the genuine flutter velocities determined in the manner.

III. Numerical Investigation and Discussion

A. Validity Test of the Present Computer Code

To demonstrate the accuracy of the present code before undergoing a series of numerical studies, two cases concerning the flutter boundaries of composite plates are examined. The results are shown in Table 3. In general, the data agree quite well with those provided by Hollowell and Dugundji.[10] It is noted that, since the aspect ratio of the tested plate is 4 (equivalent to a wing of aspect ratio 8), Hollowell and Dugundji[10] used strip aerodynamic theory and Rayleigh-Ritz method for the computation. However, for wings with more complex geometries and/or smaller aspect ratios, the present code is believed to be more appropriate because the aerodynamic model used and the finite-element discretization adopted are much more refined and general.

B. Effect of Composite Filament Angle

Plates having two different aspect ratios are chosen to study the effect of composite filament angle on the flutter and divergence behaviors. The first plate ($AR = 4$) and the second ($AR = 1.5$) represent a moderately long and a short wing, respectively. The numerical experiments were carried out while letting the composite filament angle run through the entire range of $\theta = 0$–180 deg. The result are plotted in Figs. 5 and 6. In both cases, it can be seen that the dominant instability phenomenon exhibits an alternative flutter-divergence pattern when the composite filament angle varies, as shown in

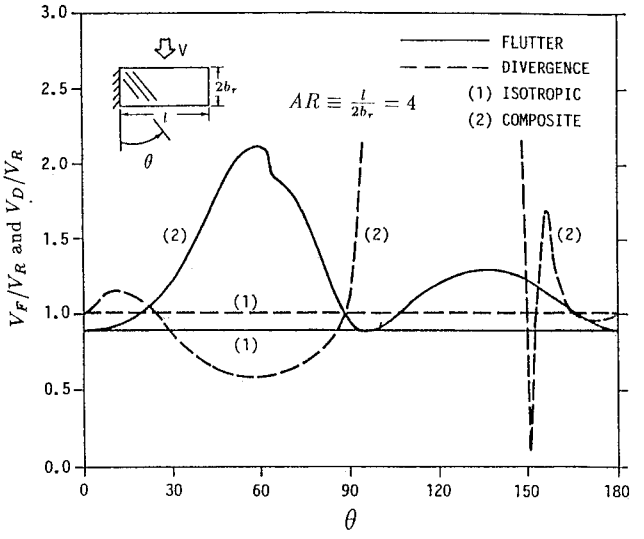

Fig. 5a Normalized flutter and divergence speeds V_F/V_R and V_D/V_R vs composite filament angle θ for $AR = 4$ ($\beta = 8$, structural mesh = 3 × 8, aerodynamic mesh = 6 × 8, $V_R = 37.809$ m/s = V_D at $\theta = 0$ deg).

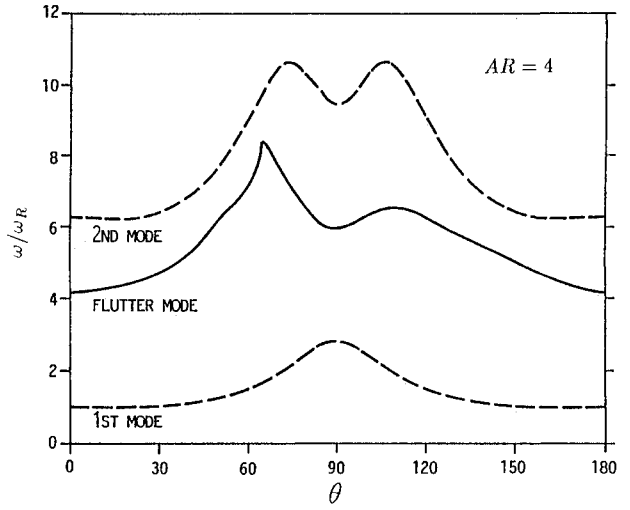

Fig. 5b Normalized flutter and natural frequencies ω/ω_R vs composite filament angle θ for $AR = 4$ ($\beta = 8$, structural mesh = 3 × 8, aerodynamic mesh = 6 × 8, $\omega_R = 1.659$ rad/s = first mode natural frequency at $\theta = 0$ deg).

Figs. 5a and 6a. The divergence-free region of the short wing ($AR = 1.5$) is found to be much narrower than that of the moderately long wing ($AR = 4$). It is noted that the present divergence trend for the moderately long wing case, except for a small range of $\theta > 150$ deg, agrees qualitatively with Weisshaar's results,[2] which were obtained by a swept beam and quasisteady aerodynamic model. Weisshaar and Ryan[29] devised a bending-torsion stiffness cross-coupling parameter to simulate the effect of composites on the aeroelastic instabilities. Using this cross-coupling parameter, they analytically discovered the phenomenon termed flutter-divergence tradeoff. The tradeoff arises from the fact that, by adjusting the directional stiffness of composites, one can only produce either a wash-in (bend up/nose up) or a wash-out (bend up/nose down) tailored structure, but not both. Wash-in is favorable for enlarging flutter and wash-out for divergence boundaries. Therefore, it is basically contradictory to obtain a structural tailoring that simultaneously achieves both high-flutter and high-divergence boundaries. The present results for plate-like wings also exhibit this tradeoff behavior—but, in a more involved manner. The tradeoff is no longer typified by a single value of cross-coupling separating the whole parameter

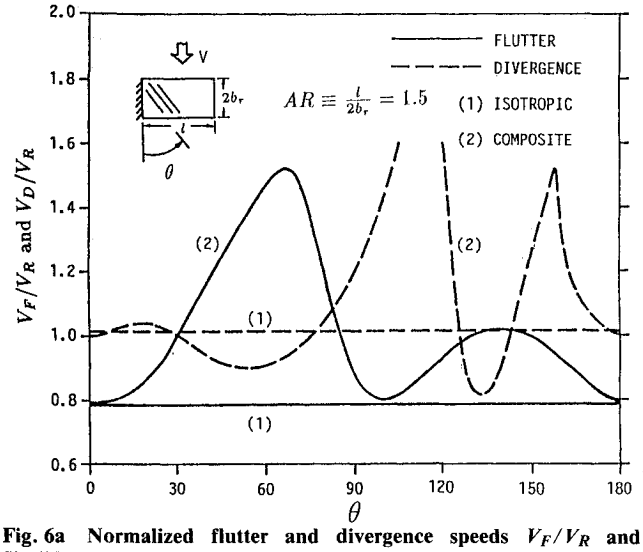

Fig. 6a Normalized flutter and divergence speeds V_F/V_R and V_D/V_R vs composite filament angle θ for $AR = 1.5$ ($\beta = 4$, structural mesh = 3 × 4, aerodynamic mesh = 5 × 5, V_R = 138.47 m/s = V_D at $\theta = 0$ deg).

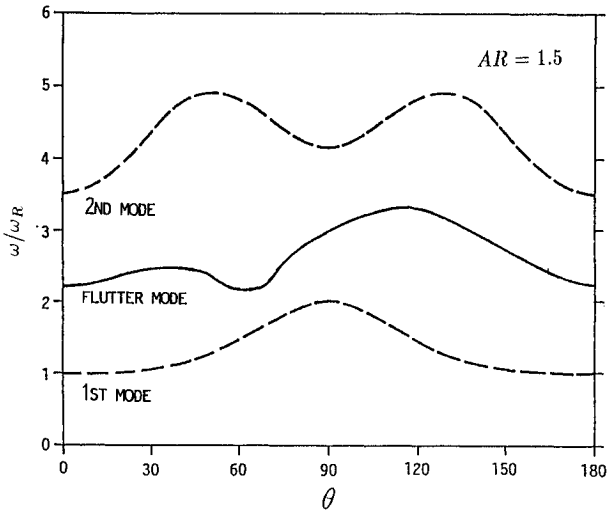

Fig. 6b Normalized flutter and natural frequencies ω/ω_R vs composite filament angle θ for $AR = 1.5$ ($\beta = 4$, structural mesh = 3 × 4, aerodynamic mesh = 5 × 5, ω_R = 11.835 rad/s = first mode natural frequency at $\theta = 0$ deg).

range into two regions bounded respectively by monotonically varying stability boundaries as illustrated in Refs. 1 and 29. Instead, for the present plate-like model, the high-flutter/low-divergence and high-divergence/low-flutter boundary zones, confined by wavy shape curves, generally appear to describe the tradeoff phenomenon. It is observed that, generally, high flutter speed occurs for $\theta < 90$ deg and high divergence for $\theta > 90$ deg. This observation complies with the previous finding that the fiber orientation shows an opposite trend compared to the effect of the wing sweep angle. As a whole, it is concluded that varying the directional stiffness could be either beneficial or detrimental for plate-like wings, and a careful parametric study is critical because the instability characteristics are complicated by the use of composite materials.

Another point worth mentioning is the asymmetry of the flutter frequency with respect to the composite orientation. The asymmetric flutter frequencies are shown in Figs. 5b and 6b where the structural natural frequencies are seen to be symmetric. This asymmetry in the flutter frequency with respect to the composite filament angle is attributed to the fact that the unsteady air load is not symmetric fore-and-aft because of the Kutta condition required at the trailing edge of the wing.

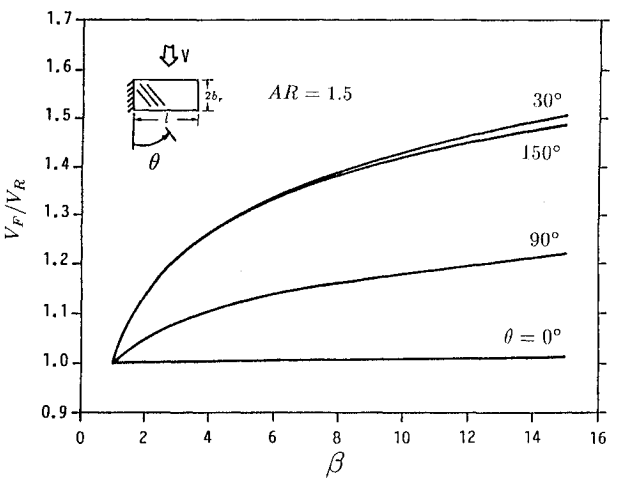

Fig. 7 Normalized flutter speeds V_F/V_R vs orthotropic modulus ratio β for $AR = 1.5$ (structural mesh = 3 × 4, aerodynamic mesh = 5 × 5, V_R = 108.7 m/s).

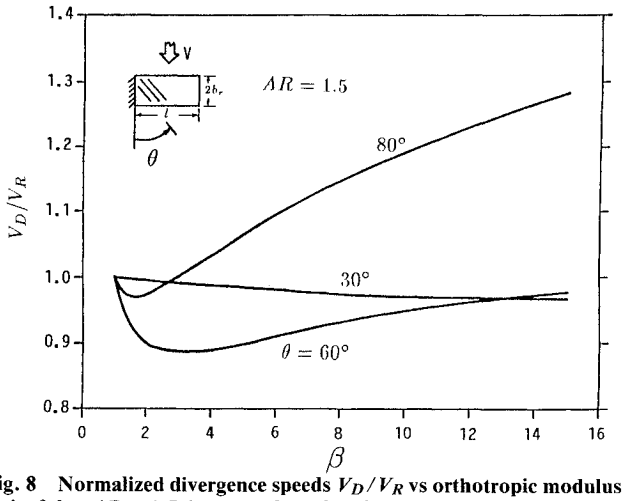

Fig. 8 Normalized divergence speeds V_D/V_R vs orthotropic modulus ratio β for $AR = 1.5$ (structural mesh = 3 × 4, aerodynamic mesh = 5 × 5, V_R = 139.99 m/s).

C. Effect of Orthotropic Modulus Ratio

Figures 7 and 8 show the effect of orthotropic modulus ratio β on the flutter and divergence boundaries of a wing with $AR = 1.5$. The values associated with the vertical coordinates are all normalized by the corresponding flutter or divergence speed of the isotropic cases. In the case of flutter (see Fig. 7), increasing β is found beneficial in enlarging the flutter boundary. Except for the case of $\theta = 0$ deg, an increasing β value may result in the increase of flutter speed, and the amount of improvement depends strongly on the filament orientation.

Figure 8 shows the case of divergence for the same wing structure examined in Fig. 7. It is seen that the change in the divergence speed is not monotone while enlarging the orthotropic modulus ratio. This phenomenon is different from what were experienced in previous examinations of flutter.

The above observations imply that the orthotropic modulus ratio, under certain filament angle orientation, could induce contradictory effects upon flutter and divergence performances. For example, in Fig. 9, which is a case of $\theta = 30$ deg, the flutter boundary increases and the divergence boundary decreases while enlarging the β value. Therefore, the optimal β value here is 4.4, which corresponds to the intersection of the two curves. Beyond $\beta = 4.4$, the low-divergence boundary will offset the gain in the flutter improvement. Therefore, a simultaneous account of the effects of the composite orthotropic modulus ratio and filament orientation is necessary for an optimal tailoring of the structures, although using

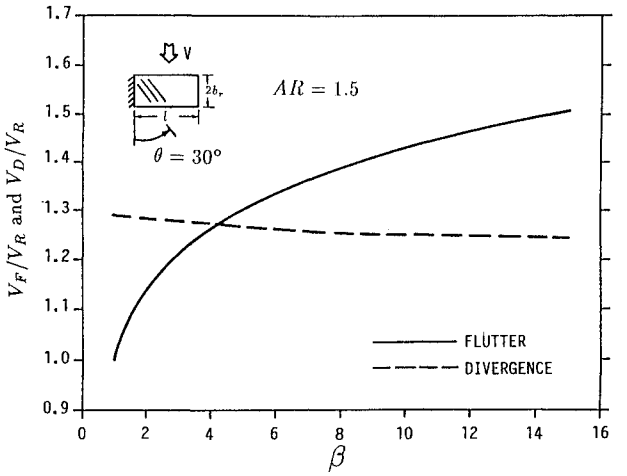

Fig. 9 Normalized flutter and divergence speeds V_F/V_R and V_D/V_R vs orthotropic modulus ratio β for $AR = 1.5$ at $\theta = 30$ deg (structural mesh = 3 × 4, aerodynamic mesh = 5 × 5, V_R = 108.7 m/s).

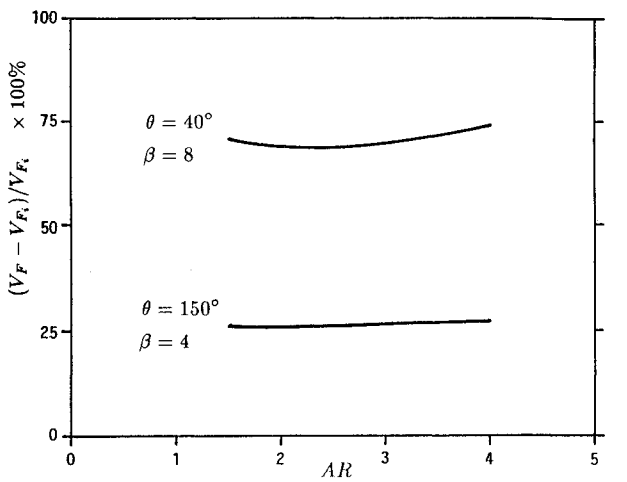

Fig. 11 Percentage increment in flutter speeds of composite wing vs the aspect ratio AR (V_{F_i} = flutter speeds of isotropic wing plotted in Fig. 10).

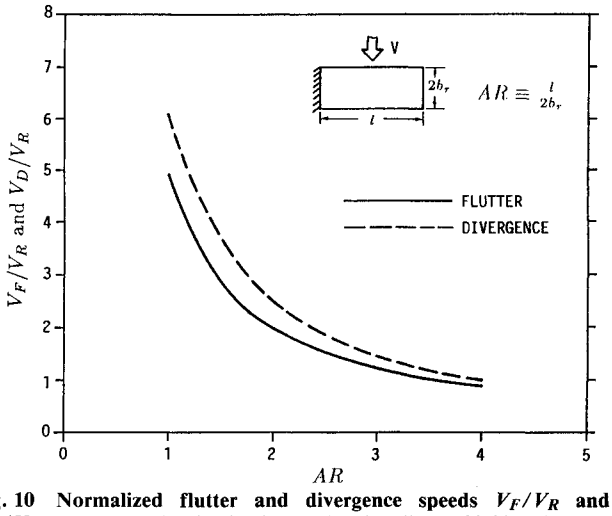

Fig. 10 Normalized flutter and divergence speeds V_F/V_R and V_D/V_R vs aspect ratio AR for isotropic wing (V_R = 38.02 m/s = V_D at $AR = 4$).

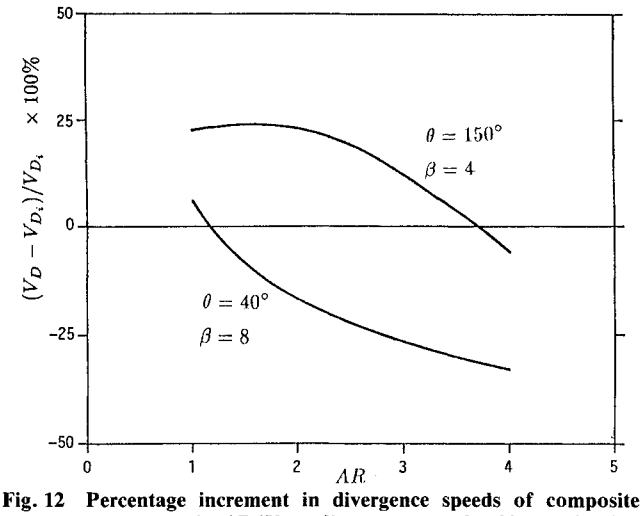

Fig. 12 Percentage increment in divergence speeds of composite wing vs the aspect ratio AR (V_D = divergence speeds of isotropic wing plotted in Fig. 10).

composites can provide a latitude for improving the flutter and divergence performances.

D. Effect of Aspect Ratio

In Figs. 10–12, the effects of aspect ratio AR on the flutter and divergence boundaries are illustrated for both isotropic and composite cantilevered plates. Figure 10 shows the isotropic case ($\beta = 1$) where the flutter and divergence speeds are normalized by the divergence speed at $AR = 4$. It is seen that both the flutter and divergence speeds increase monotonically as AR decreases. The increasing rates of flutter and divergence speeds are substantial when AR is less than 1.5.

For composite wings, the percentage increments of flutter and divergence speeds over the isotropic wing are plotted in Figs. 11 and 12, respectively. It is found that the flutter increments due to the use of composites are usually significant and less sensitive with respect to the AR value (see Fig. 11). However, the divergence increments, as shown in Fig. 12, may become negative with the increasing value of the aspect ratio. Moreover, the occurrence of the negative divergence increment is seen to be pretty parametrically dependent upon both the composite filament angle and the orthotropic modulus ratio.

E. Effect of Sweep Angle

It is known that forward- or backward-swept wings exhibit different types of instabilities. Making wings sweep forward will result in a structural wash-in, which in general lowers the divergence boundaries. For swept-back wings, however, the flutter boundaries become lower owing to the associated structural wash-out. The use of composite tailoring, by increasing the wash-out or wash-in through the adjustment of the fiber filament orientation, can provide a balance between the flutter and divergence speeds.

The numerical experiment showing the sweep angle effect, as illustrated in Fig. 13, is performed for a low-aspect-ratio wing, $AR = 1.5$. The sweep angle Λ is changed by rotating the wing structure while keeping the wing area invariant (a schematic is depicted in the upper left corner of Fig. 13). Two cases are tested, at $\theta = 40$ and 105 deg, which respectively represent the forward and backward swept of the composite filament angle. The former tends to increase the wing wash-in while the latter increases the wash-out. Therefore, in Fig. 13 it can be seen that the $\theta = 40$ deg case shows a lower divergence speed for $\Lambda < 0$, but higher flutter speed for $\Lambda > 0$, and vice versa for the $\theta = 105$ deg case. It can be concluded that using composite tailoring can achieve a harmonious compensation to recover, to some degree, the stability deficit caused by the wing sweep angle.

IV. Concluding Remarks

This paper presents a computational method for solving flutter/divergence problems associated with composite wings. The high-precision triangular plate bending finite-element discretization and the doublet-lattice method of unsteady subsonic aerodynamics are used for the structural and aerodynamic models, respectively. A computer program based on this framework is developed and checked with the existing experimental and computational results from other sources.

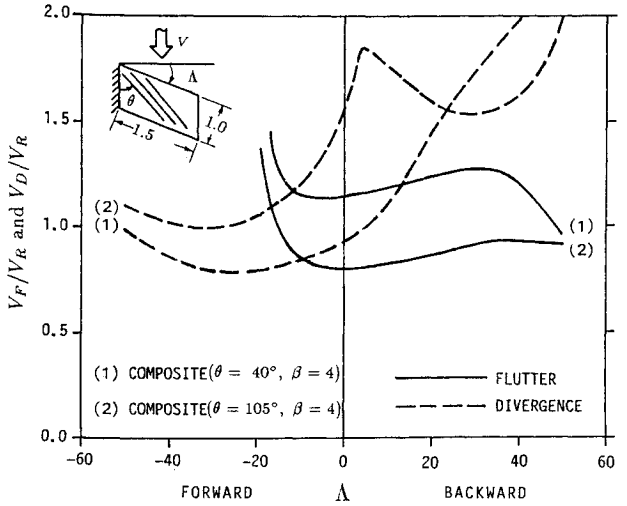

Fig. 13 Normalized flutter and divergence speeds V_F/V_R and V_D/V_R vs sweep angle for the composite wing.

Excellent agreements in both the free-vibration and flutter examinations are obtained to indicate that the present method is quite accurate.

Parametric studies are also performed to investigate the effects of composite filament angle, orthotropic modulus ratio, aspect ratio, and sweep angle on the flutter/divergence behavior of a plate-like structure. For low-aspect-ratio wings, the flutter/divergence tradeoff is still observed, but in a more involved manner. As the composite filament angle changes, the flutter and divergence trends show a wavy shape variation, approximately with the 90 deg of phase shift that typifies the tradeoff phenomenon of finite wings. The orthotropic modulus ratio may effectively enhance the flutter performance, but a reversed effect on divergence has been found for some filament angle orientations. As for the aspect ratio effect, the flutter improvement gained by the use of composites shows a consistent trend as the aspect ratio increases. Nevertheless, this is not true for the divergence performance. A large aspect ratio tends to offset the gain in divergence provided by composites and the situation deteriorates as the aspect ratio gets larger. The results of a study of the wing sweep angle effect confirm that structural tailoring can provide a harmonious balance to the sweep angle effect on the stability characteristics of the wing. In all, significant improvement upon flutter/divergence characteristics can be achieved by using composite materials so long as the structures considered are properly tailored.

It is emphasized that the present work is primarily a methodology development. Extensions to more complex configurations of structures can readily be made in order to study some other effects, such as wing planform, rigid-body modes, and control surfaces, on the flutter of a composite wing in subsonic flow.

Acknowledgments

This work was supported by National Science Council under Contract CS76-0210-D006-14. The authors would like to thank Dr. Yuan-Bin Chang of Aeronautical Research Laboratory for many valuable discussions.

References

[1]Shirk, M., Hertz, T. J., and Weisshaar, T. A., "Aeroelastic Tailoring-Theory, Practice, and Promise," *Journal of Aircraft,* Vol. 23, Jan. 1986, pp. 6-18.

[2]Weisshaar, T. A., "Divergence of Forward Swept Composite Wings," *Journal of Aircraft,* Vol. 17, June 1980, pp. 442-448.

[3] Weisshaar, T. A., "Aeroelastic Tailoring of Forward Swept Composite Wings," *Journal of Aircraft,* Vol. 18, Aug. 1981, pp. 669-676.

[4]Sherrer, V. C., Hertz, T. J., and Shirk, M. H., "Wind Tunnel Demonstration of Aeroelastic Tailoring Applied to Forward Swept Wings," *Journal of Aircraft,* Vol. 18, Nov. 1981, pp. 976-983.

[5]Blair, M. and Weisshaar, T. A., "Swept Composite Wing Aeroelastic Divergence Experiments," *Journal of Aircraft,* Vol. 19, Nov. 1982, pp. 1019-1024.

[6]Lehman, L. L., "A Hybrid State Vector Approach to Aeroelastic Analysis," *AIAA Journal,* Vol. 20, Oct. 1982, pp. 1442-1449.

[7]Lottati, I., "Flutter and Divergence Aeroelastic Characteristics for Composite Forward Swept Cantilevered Wings," *Journal of Aircraft,* Vol. 22, Nov. 1985, pp. 1001-1007.

[8]Rogers, W. A., Braymen, W. W., and Shirk, M. H., "Design, Analyses, and Model Tests of an Aeroelastically Tailored Lifting Surface," *Journal of Aircraft,* Vol. 20, March 1983, pp. 208-215.

[9]Braymen, W. W., Rogers, W. A., and Shirk, M. H., "Wind Tunnel Test and Aerodynamic Analysis of Three Aeroelastically Tailored Wings," *Proceedings of the 13th Congress of International Council of the Aeronautical Sciences and AIAA Aircraft Systems and Technology Conference,* ICAS-82-5.7.3., Aug. 1981.

[10]Hollowell, S. J. and Dugundji, J., "Aeroelastic Flutter and Divergence of Stiffness Coupled, Graphite/Epoxy Cantilevered Plates," *Journal of Aircraft,* Vol. 21, Jan. 1984, pp. 69-76.

[11]Landsberger, B. J. and Dugundji, J., "Experimental Aeroelastic Behavior of Unswept and Forward-Swept Cantilever Graphite/Epoxy Wings," *Journal of Aircraft,* Vol. 22, Aug. 1985, pp. 679-686.

[12]Argyris, J. H., Fried, I., and Scharpf, D. W., "The TUBA Family of Plate Elements for the Matrix Displacement Method," *Aeronautical Journal of the Royal Aeronautical Society,* Vol. 72, No. 692, Aug. 1968, pp. 701-709.

[13]Bell, K., "A Refined Triangular Plate Bending Finite Element," *International Journal for Numerical Methods in Engineering,* Vol. 1, Jan.-March 1969, pp. 101-122.

[14]Cowper, G. R., Kosko, E., Lindberg, G. M., and Olson, M. D., "Static and Dynamic Applications of a High- Precision Triangular Plate Bending Element," *AIAA Journal,* Vol. 7, Oct. 1969, pp. 1957-1965.

[15]Stavitsky, D., Macagno, E., and Christensen, J., "On the Eighteen Degrees of Freedom Triangular Element," *Computer Methods in Applied Mechanics and Engineering,* Vol. 26, No. 3, Sept. 1981, pp. 265-283.

[16]Jeyachandrabose, C. and Kirkhope, J., "Explicit Formulation for the High Precision Triangular Plate-Bending Element," *Computers and Structures,* Vol. 19, No. 4, 1984, pp. 511-519.

[17]Jeyachandrabose, C. and Kirkhope, J., "Explicit Formulation for a High Precision Triangular Laminated Anisotropic Thin Plate Finite Element," *Computers and Structures,* Vol. 20, No. 6, 1985, pp. 991-1007.

[18]Tsai, S. W. and Hahn, H. T., *Introduction to Composite Materials,* Technomic Pub., Westport, CT, 1980, Chap. 6.

[19]Lottati, I., "The Role of Structural and Aerodynamic Damping on the Aeroelastic Behavior of Wings," *Journal of Aircraft,* Vol. 23, July 1986, pp. 606-608.

[20]Bolotin, V. V. and Zhinzher, N. I., "Effects of Damping on Stability of Elastic Systems Subjected to Nonconservative Forces," *International Journal of Solids and Structures,* Vol. 5, Sept. 1969, pp. 965-989.

[21]Landahl, M. T., "Kernel Function for Nonplanar Oscillating Surfaces in a Subsonic Flow," *AIAA Journal,* Vol. 5, May 1967, p. 1045.

[22]Chu, S. and Lu, P. J., "Simplified Calculation Method for Subsonic Airloads on Wing-Body Combinations," *Proceedings of the National Science Council, Republic of China,* Vol. 3, No. 2, April 1979, pp. 212-221.

[23]Lu, P. J., "Investigation of the Interference between Non-Planar Lifting-Surfaces and Slender Body in Unsteady Subsonic Flow," M.S. Thesis, National Taiwan Univ., Taipei, Taiwan, 1978.

[24]Albano, E. and Rodden, W. P., "A Doublet-Lattice Method for Calculating Lift Distributions on Oscillating Surfaces in Subsonic Flows," *AIAA Journal,* Vol. 7, Feb. 1969, pp. 279-285.

[25]Lessing, H. C., Troutman, J. L., and Menees, G. P., "Experimental Determination of the Pressure Distribution on a Rectangular Wing Oscillating in the First Bending Mode for Mach Numbers from 0.24 to 1.30," NASA TN D-344, 1960.

[26]Harder, R. L. and Desmarais, R. N., "Interpolation Using Surface Splines," *Journal of Aircraft,* Vol. 9, Feb. 1972, pp. 189-191.

[27]Lin, K. J., "Flutter Analysis of Composite Plates with Patched Cracks," Ph.D. Dissertation, Institute of Aeronautics and Astronautics, National Cheng Kung Univ., Tainan, Taiwan, July 1988.

[28]Srinivasan, R. S. and Babu, B. J. C., "Free Vibration of Cantilever Quadrilateral Plates," *Journal of the Acoustical Society of America,* Vol. 73, March 1983, pp. 851-855.

[29]Weisshaar, T. A. and Ryan, R. J., "Control of Aeroelastic Instabilities Through Stiffness Cross-Coupling," *Journal of Aircraft,* Vol. 23, Feb. 1986, pp. 148-155.